

Laser intensity effects in carrier-envelope phase-tagged time of flight-photoemission electron microscopy

S. H. Chew^{1,2} · A. Gliserin^{1,2} · J. Schmidt¹ · H. Bian¹ · S. Nobis¹ · F. Schertz³ · M. Kübel² · Y.-Y. Yang⁴ · B. Loitsch⁵ · T. Stettner⁵ · J. J. Finley⁵ · C. Späth^{1,2} · H. Ouacha⁶ · A. M. Azzeer⁶ · U. Kleineberg¹

Received: 17 August 2015 / Accepted: 25 February 2016 / Published online: 12 April 2016
© The Author(s) 2016. This article is published with open access at Springerlink.com

Abstract A time of flight-photoemission electron microscope is combined with a single-shot stereographic above-threshold ionization phase meter for studying attosecond control of electrons in tailored plasmonic nanostructures spatially and energetically via a carrier-envelope phase tagging technique. First carrier-envelope phase-resolved measurements of gold nanoparticles on gold plane and surface roughness from a gold film show an apparent carrier-envelope phase modulation with a period of π . This modulation is found to originate from an intensity dependence of the photoelectron spectra and the carrier-envelope phase measurement rather than from an intrinsic carrier-envelope phase dependence, which is confirmed by simulations. This useful finding suggests that intensity tagging should be considered for phase tagging experiments on plasmonic nanostructures with low carrier-envelope phase sensitivity

in order to correct for the intensity-related carrier-envelope phase artifact.

1 Introduction

The vast progress in the development of few-cycle optical laser pulses during the last few years has enabled new types of ultrafast experiments such as carrier-envelope phase (CEP)-sensitive measurements aiming to steer electron motion on ultrashort timescales and nanometer spatial resolutions. Ti:sapphire amplifiers in combination with a pulse compressor system based on nonlinear spectral broadening (e.g., in a fiber) and enhanced dispersion control are able to provide few-cycle pulses in the low mJ range at kHz repetition rates [1, 2] and are the prominent sources to date. These pulses may contain less than two optical field cycles, and the electric field strength considerably changes after one optical cycle constituting the breakdown of the slowly varying envelope approximation valid for multicycle pulses. Hence, the phase of the electric field with respect to its envelope (referred to as CEP) starts to play an important role in light–matter interactions and strongly affects any nonlinear optical processes, which depend on the instantaneous field strength rather than on the intensity. As the CEP of an ultrashort wavepacket from a laser generally experiences random fluctuations from shot to shot, methods to stabilize it have been developed [3, 4], which led to the generation of frequency combs [5] and isolated attosecond pulses [6, 7], for instance. CEP effects have already been demonstrated on gases [8–10], molecules [11, 12] and solids [13–16], providing a basic insight into light–matter interactions and revealing its enormous potential to precisely manipulate and control ultrafast electron dynamics. In the meantime, surface plasmon polariton-assisted

This article is part of the topical collection “Ultrafast Nanooptics” guest edited by Martin Aeschlimann and Walter Pfeiffer.

✉ S. H. Chew
SooHoon.CheW@mpq.mpg.de

- ¹ Faculty of Physics, Ludwig Maximilian University of Munich, 85748 Garching, Germany
- ² Max Planck Institute of Quantum Optics, 85748 Garching, Germany
- ³ Surface Concept GmbH, Staudingerweg 7, 55128 Mainz, Germany
- ⁴ Laboratory of All Solid State Light Sources, Institute of Semiconductors, Qinghua East Road 35a, Haidian District, Beijing 100083, People’s Republic of China
- ⁵ Walter Schottky Institute and Physics Department, Technical University of Munich, 85748 Garching, Germany
- ⁶ King Abdullah Institute for Nanotechnology, King Saud University, Riyadh 12373, Saudi Arabia

photoemission has attracted a lot of attention [17–19] and recently strong CEP dependence of the photocurrent from metal nanotips has been demonstrated [15, 20]. Hence, it is very interesting to study the CEP dependence of engineered nanostructures with different designs and shapes.

Photoemission electron microscopy (PEEM) is a well-developed surface science tool and can be used in a wide range of applications from visualizing metals to biological samples with subwavelength spatial resolution. PEEM is becoming increasingly important for studying ultrafast phenomena and processes in magnetic domain structures [21–23]. A number of significant developments have also been dedicated to the study of nonlinear photoemission [24] and ultrafast time-resolved surface plasmon dynamics in nanostructures [25–29] by using PEEM in combination with femtosecond and attosecond laser sources more than a decade ago. Previously, we have initiated and proposed the attosecond plasmonic field microscope [30–32] for a direct and noninvasive access to the plasmonic dynamics in nanostructured surfaces with attosecond temporal and nanometer spatial resolution. In the initial work, we have demonstrated that a spatial resolution of ~ 200 nm could be achieved using ~ 350 as extreme ultraviolet pulses on lithographically fabricated gold structures. We have further shown that utilizing energy-filtered imaging of the secondary electrons could improve the chromatic aberrations, and we have also successfully proven the microspectroscopic identification of core and valence band electronic states using these ultrashort extreme ultraviolet pulses [30]. However, it is more intriguing to use the CEP of few-cycle laser pulses to control the plasmonic optical fields besides probing them with our proposed attosecond plasmonic field microscope. Instead of employing a typical commercially available CEP locking scheme [33–35], we have combined single-shot phase tagging with time of flight-photoemission electron microscopy (ToF-PEEM) for controlling and probing plasmonic fields. Single-shot phase tagging utilizes a stereographic above-threshold ionization (ATI) phase meter [36–38] to detect ATI electrons of xenon (Xe) for CEP determination, which is an alternative technique to CEP locking. Phase tagging offers several advantages over CEP locking, i.e., omitting the need of precise phase stabilization, permitting real-time determination of CEP for every single laser shot and continuous real-time monitoring of laser performance. Moreover, this technique enables parallel data acquisition for all CEPs within a certain measurement time, which evenly distributes any possible dynamic changes during the measurement, e.g., sample drift, over all CEP values. In contrast, CEP locking requires a serial scan, where drift of the experimental parameters correlates with the scanned CEP, leading to systematic errors. Phase tagging also allows for long data acquisition times over several hours and even over more than 10 h with a correction

scheme [39]. Therefore, this technique is suitable for our experimental setup, since long acquisition times are required to compensate for the low count rate due to limited available laser intensities in order to avoid undesirable space charge effects.

In this work, we have performed the first experiments using our newly developed CEP-tagged ToF-PEEM to investigate the CEP effects from plasmonic samples. We found that the CEP effects from the plasmonic nanostructures can possibly be overshadowed by an undesirable CEP artifact, which is correlated to laser intensity fluctuations. Therefore, we carried out intensity-dependent measurements on the kinetic energy of photoelectrons emitted from hot spot areas of the plasmonic sample and the CEP of the according laser pulses detected by the stereographic ATI phase meter to gain a deeper understanding to explain this CEP artifact. Our findings, which are supported by simulations, give a new insight that intensity-biased CEP detection by the phase meter could indeed affect real CEP retrieval for the low CEP sensitivity of photoemission processes from metallic surfaces [13, 14, 40] and an ensemble of inhomogeneous nanostructures [41]. Our work here paves the way to precise measurements of CEP control on plasmonic nanostructures using CEP-tagged ToF-PEEM for ultrahigh spatiotemporal resolution.

2 Experimental setup

The setup for combining a single-shot ToF-PEEM with a stereographic ATI phase meter is schematically illustrated in Fig. 1a. Data acquisition of both the stereographic ATI phase meter and the ToF-PEEM is synchronized to broadband few-cycle laser pulses in order to enable single-shot phase tagging measurements. The experiments were performed using few-cycle laser pulses with a central wavelength of 730 nm at a repetition rate of 10 kHz. Few-cycle laser pulses as short as 4–6 fs were obtained after hollow-core fiber compression by means of self-phase modulation followed by an appropriate chirp compensation (see Fig. 1a). Figure 1b depicts the broadband hollow-core fiber spectrum ranging from 400 nm to 1000 nm with a central wavelength of 730 nm. The pulse energy achieved after the hollow-core fiber compression is 160 μ J. One part of the few-cycle laser pulses, containing 70 % of the pulse energy, is focused into a Xe gas target inside the stereographic ATI phase meter using a 250-mm focal length spherical mirror, while the remaining part is directed into the ToF-PEEM chamber. A typical parametric asymmetry plot (PAP) obtained with our stereographic ATI phase meter is shown in Fig. 1c. The laser pulse length can be determined from the radius of the PAP [37]. Individual pairs of fused silica wedges are used in the beam paths to correct for residual

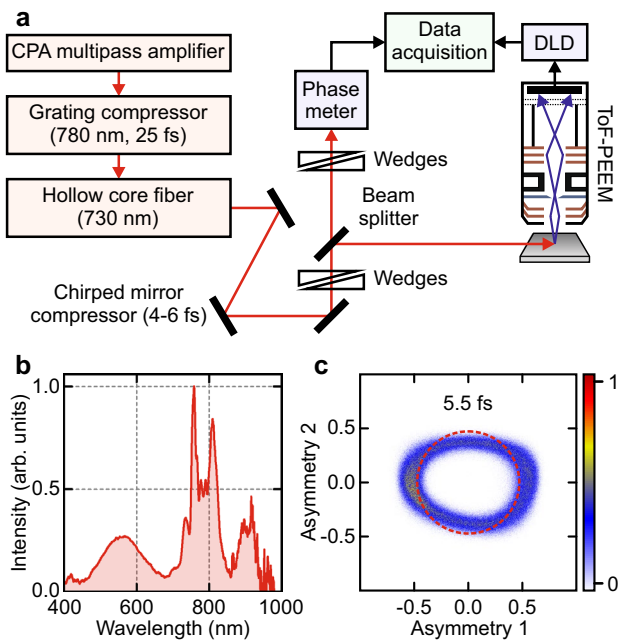


Fig. 1 Schematic view of the CEP-tagged ToF-PEEM setup. **a** The 10-kHz commercial Ti:sapphire laser system (Femtowatt Compact Pro, Femtolasers GmbH) is designed based on a multipass chirped pulse amplification (CPA) concept. The 25-fs amplified pulses are then compressed by a grating compressor. The laser spectrum is then broadened by an argon-filled hollow-core fiber via self-phase modulation. Few-cycle laser pulses as short as 4–6 fs (bandwidth limited) are achieved after the chirped mirror compression. A beam splitter directs one laser beam to the phase meter and one to the ToF-PEEM, respectively. The pulse duration for the phase meter and ToF-PEEM can be optimized individually by the respective wedge insertion. **b** Hollow-core fiber spectrum which has a central wavelength of 730 nm. **c** A typical PAP showing a pulse duration of 5.5 fs recorded by the phase meter. The *colorbar* shows the counts

chirp in order to ensure shortest pulses and irises are used to vary the laser intensity in both instruments.

The ToF-PEEM (30 kV version of FOCUS IS-PEEM, FOCUS GmbH) consists of a ToF detector and a complementary imaging energy filter (IEF), which is a high-pass retarding field analyzer, both integrated in a straight column for simple handling [31]. The ToF option inside the PEEM is advantageous for time-resolved imaging at low count rates, whereas the IEF provides time-integrated and energy-filtered images for high-intensity applications. The ToF option is realized by a drift tube followed by a retractable delayline detector (DLD-3636, Surface Concept). We solely used the DLD instead of the IEF for the energy-resolved experiments described in this work for two main reasons: First, the DLD is capable of synchronized single-shot operation, which is essential for phase tagging of every laser-triggered event, and second, the DLD has a superior signal-to-noise ratio [42], which enables low count rate detection, as low laser intensity was used here in order

to suppress space charge effects. For the implementation of the phase tagging, we have modified the time-to-digital converter of the DLD and used a custom made firmware to correlate each count detected by the DLD to a particular laser shot that triggered that count. This provides an absolute timing between each detected DLD count and the corresponding laser pulse. A hardware-triggered data acquisition system ensures a synchronized start of both the DLD and the phase meter, which are then clocked by the 10-kHz laser pulses via photodetectors. A constant fraction discriminator is used to transform the electric pulses from the photodetector into transistor-transistor logic pulses suitable for the time-to-digital converter. The data from the DLD and the phase meter are simultaneously recorded by a computer program, which correlates the photoelectron counts from the DLD to the CEP of the corresponding laser shots.

With this ToF-PEEM setup, we could achieve a spatial resolution of ~ 25 nm using a copper-coated silicon microstructure test sample in a threshold photoemission mode using ultraviolet (UV) excitation. In addition, we demonstrated an energy resolution of ~ 50 meV using a Mo(110) crystal with two-photon photoemission characterization [31]. For the CEP-tagged PEEM experiments, we used a mercury arc lamp (unpolarized continuous wave UV source) for sample imaging and alignment prior to the few-cycle laser excitation of the samples. The incidence angle of both the UV light and the p-polarized laser pulses was 65° to the sample surface normal. In order to reduce too high peak intensity on the sample due to intense few-cycle laser pulses, the focusing mirror ($f = 250$ mm) was positioned such that the defocused beam spot onto the sample was rather big, approximately $300 \mu\text{m} \times 600 \mu\text{m}$. The experiments were conducted under ultrahigh vacuum conditions with a pressure of $\sim 10^{-9}$ mbar.

The CEP of every laser pulse can be determined via a relatively new but well-established technique, single-shot phase tagging using a stereographic ATI phase meter [36–38, 43, 44]. In short, two ToF spectra of the CEP-sensitive rescattered ATI electrons with high energy emitted from the Xe are recorded on both left and right microchannel (MCP) detectors placed along the polarization axis of the focused laser beam. The ToF spectra yielding the ATI electron spectra are detected as time-dependent electron currents at the MCP detectors and are converted into time-dependent voltages. In order to retrieve the CEP in real-time from the ToF spectra, two properly adjusted gated integrations are applied to the ToF spectra for each laser shot. Two asymmetry values, $A_{1,2} = (L_{1,2} - R_{1,2}) / (L_{1,2} + R_{1,2})$ can be calculated using an electronic circuit where L and R are the integrated electron yields of the left and right MCP detectors, respectively. Next, a PAP of A_1 and A_2 can be generated, in which the polar angle, θ , corresponds to the CEP, φ , of the laser pulse via the relation $\theta \approx \varphi + \varphi_0$, where φ_0 is an

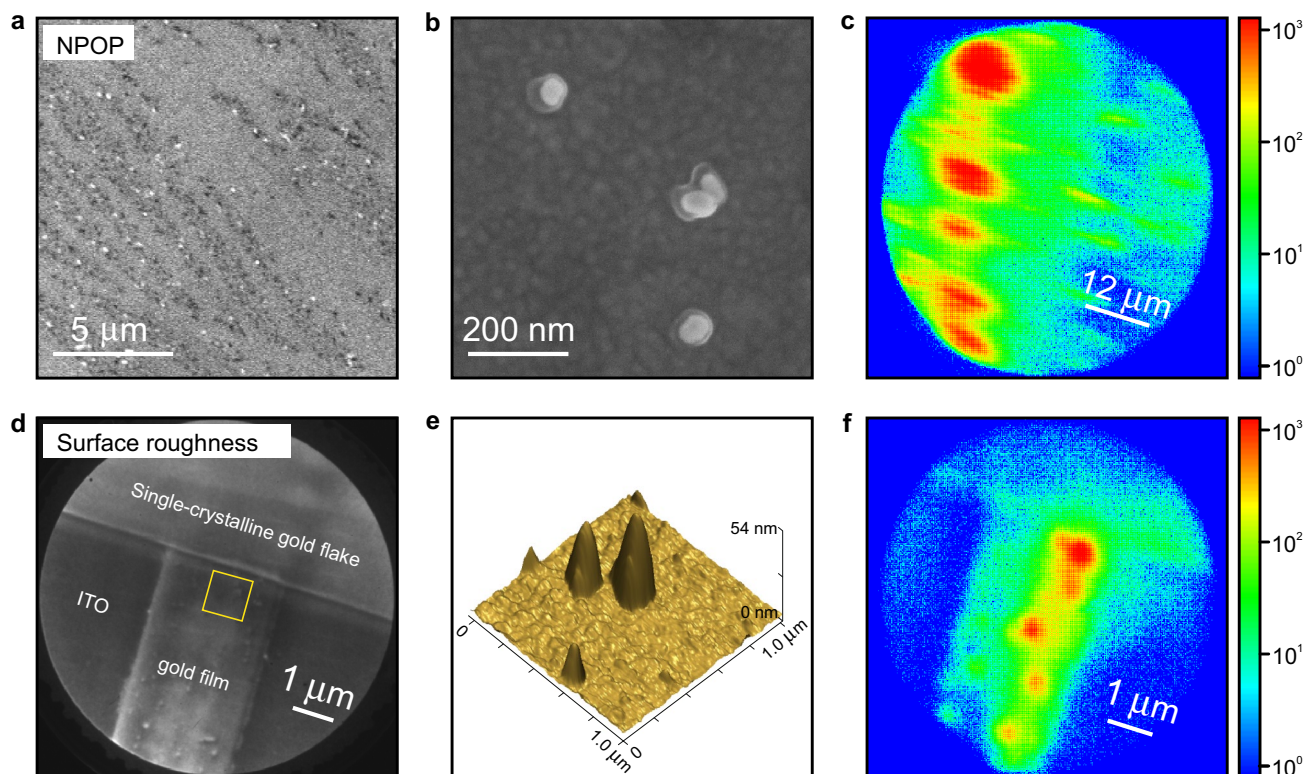


Fig. 2 Microscopic images of NPOP and gold surface roughness samples. **a** SEM image of the NPOP showing isolated gold nanoparticles indicated by the *bright dots* on the gold film surface. **b** A zoomed-in SEM image of the ~ 90 -nm gold nanoparticles. **c** PEEM image of NPOP illuminated by few-cycle laser pulses. The hot spots are from plasmonic-enhanced photoemission of the nanoparticles. Larger hot spots are formed by clustered nanoparticles. The *colorbar* shows the counts. **d** PEEM image of the 90-nm-thick multicrystalline gold film on ITO-coated glass substrate using UV lamp excitation.

The surface roughness of <1 -nm rms is too fine to be resolved with the PEEM. However, a larger surface roughness of ~ 11 nm rms can be seen on the gold film surface. **e** AFM image of the area marked by a *yellow square* in **d**. Two kinds of surface roughness are observed, see text for details. **f** PEEM image of the same sample area as shown in **d**, acquired with few-cycle laser pulses. The hot spots originate from plasmonic-enhanced photoemission from the gold surface roughness. The *colorbar* shows the counts

arbitrary offset. Hence, the CEP, φ , of each laser pulse can be determined exactly, since the laser produces randomly and uniformly distributed CEP values, although there is a small deviation between the dependence of θ and φ [45]. These asymmetry values are recorded simultaneously with the DLD photoelectron counts, therefore enabling phase tagging of every detected event in the experiment.

3 Results and discussion

We performed first CEP-tagged PEEM experiment on gold nanoparticles on gold plane (NPOP) with a subnanometer gap [46–48] via a multiphoton photoemission process. A very thin layer of the organic molecule cysteamine serves as a spacer or gap between these gold nanoparticles (~ 90 nm average diameter) and a 50-nm-thick gold film. NPOP exhibits a very strong field enhancement when in resonance, since they have a very small but well-defined

gap size, smaller than 1 nm. Figure 2a, b depicts the NPOP at medium magnification and high magnification, respectively, under a scanning electron microscope (SEM). A field enhancement factor of ~ 400 is obtained based on finite element method simulations using our laser excitation parameters. A defocused peak laser intensity of $\sim 5 \times 10^8$ W/cm² was used to illuminate the sample. Figure 2c shows the energy-integrated PEEM image over 7×10^6 laser shots on the NPOP sample. The image is smeared out in one direction because astigmatism was not corrected during the measurement. Figure 3a, b illustrates the corresponding integrated electron energy spectrum from the entire PEEM image (60 μ m field of view) and a PAP obtained from the phase meter, respectively. The PAPs shown in Fig. 3 are reconstructed from the phase-tagged data sets. In Fig. 3a, the electron spectrum represents the kinetic energy distribution of electrons after multiphoton photoemission, reduced by the work function of the sample. It is expected that different numbers of photons are involved in the emission

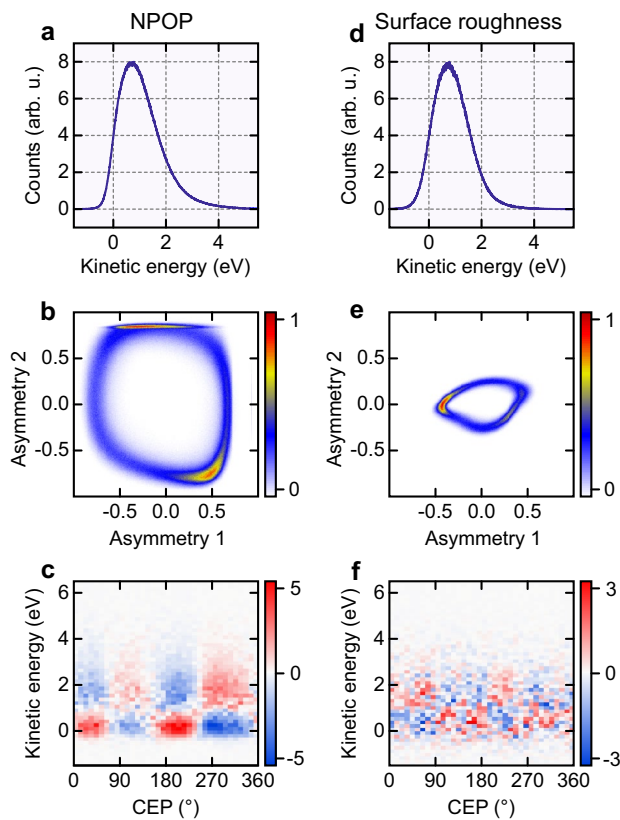


Fig. 3 CEP-tagged ToF-PEEM results on NPOP and gold surface roughness samples. **a** Normalized energy spectrum integrated over the whole NPOP sample area as shown in Fig. 2c. **b** PAP for $\sim 7 \times 10^6$ laser shots; the pulse duration is estimated as 4.1 fs. The *colorbar* shows the counts. **c** Normalized CEP spectrogram for the NPOP with the averaged spectrum subtracted. The *colorbar* represents the modulation depth in percent. **d** Normalized energy spectrum integrated over the whole surface roughness sample area as shown in Fig. 2f. **e** PAP for $\sim 2 \times 10^6$ laser shots; the pulse duration is estimated as 6.5 fs. The *colorbar* shows the counts. **f** Normalized CEP spectrogram for the gold surface roughness with the averaged spectrum subtracted. The *colorbar* represents the modulation depth in percent

process, since a broadband laser was used for excitation. In order to analyze the CEP dependence, the difference between CEP-resolved electron spectra and the CEP-averaged electron spectrum, normalized to the peak amplitude of the CEP-averaged spectrum, is taken to enhance the CEP effect and depict the modulation depth. It is shown as a CEP spectrogram in Fig. 3c. A modulation of the spectrum with a period of π is clearly visible, corresponding to an apparently CEP-dependent energy shift: The modulation of the high-energy part of the spectrum around the CEP-averaged central energy peak is inverted, i.e., shifted by π , compared to the low-energy part, while no modulation is visible at the central energy. For comparison, we also carried out a phase-tagged measurement on a 90-nm-thick multicrystalline gold film on a tin-doped indium oxide (ITO)-coated

glass substrate. Figure 2d shows the gold film feature under UV light excitation obtained with the PEEM. Irregularities, such as bigger crystal grains or possibly unknown particles on the multicrystalline gold film surface, can be observed, whereas very smooth surfaces are visible on the ITO-coated glass and single-crystalline gold flake. It is well known that evaporated multicrystalline gold films exhibit a typical diameter of crystal grains of 30–50 nm [49]. Atomic force microscope (AFM) imaging on the investigated gold film confirms a crystal grain size of 30–50 nm in our case. Its corresponding root mean square (rms) surface roughness is ~ 0.9 nm. It is intriguing to see some bigger crystal grains or unknown hill-shaped particles, which are ~ 15 –60 nm in height and have a lateral extent of ~ 50 –150 nm in the AFM image (see Fig. 2e). These irregularities result in a rms surface roughness of ~ 11.1 nm, and it is believed that the rough distinct features can be caused by coalescence or contamination either during the gold evaporation process or during the lift-off process in electron beam lithography. The photoemission from hot spots formed by the surface roughness of this gold film is shown in Fig. 2f. A defocused peak laser intensity of $\sim 8 \times 10^8$ W/cm² was used for the sample illumination. A variety of surface plasmon modes seen as the hot spots can be excited in the nanoscale gaps between gold crystal grains upon the broadband laser excitation ranging from 400 nm to 1000 nm. The integrated electron spectrum of these hot spots is depicted in Fig. 3d, and the corresponding PAP and CEP spectrogram are shown in Fig. 3e, f, respectively. When comparing the electron spectra of gold surface roughness and NPOP (see Fig. 3a, d), the NPOP exhibits a slightly higher electron kinetic energy (~ 3 –5 eV) than the surface roughness, even though the laser peak intensities for both samples are comparable. This can be explained by an energy gain of the electrons when being expelled from the strong plasmonic near-field region inside the gap, following the ponderomotive force [50]. It is believed that a weak tunnel ionization process is also involved besides the multiphoton photoemission process in the case of NPOP. Using our experimental parameters with the laser peak intensity being 5×10^8 W/cm², the sample work function being 4 eV, the central laser wavelength being 730 nm and a field enhancement of 400, we obtain a Keldysh parameter [51] of $\gamma \approx 0.87$ (photoemission is favored for $\gamma \gg 1$ and tunneling ionization for $\gamma \ll 1$). A smaller PAP is obtained for this measurement, suggesting a longer pulse duration possibly due to a change in dispersion of the laser pulses. The non-uniform shape of the PAP is caused by imperfect phase meter alignment. For the gold surface roughness sample, a similar spectral feature with a modulation period of π but with smaller modulation depth is observed (see Fig. 3f). Surprisingly, the CEP modulation remains after shifting the tagged CEP list by several events. This is not expected, since the CEP is assumed to

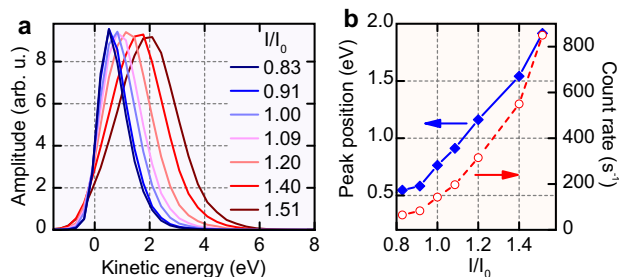


Fig. 4 Laser intensity dependence of the photoemission spectra. **a** Photoemission spectra from the gold surface roughness sample at different relative intensities (I/I_0), I_0 being the intensity used for phase-tagged experiments. Energy shift and broadening is evident. **b** Shift of the central energy as a function of intensity (blue) shows a nearly linear intensity dependence after an *onset*. The count rate increases with an exponent of 4.4 as a function of intensity (red), indicating a 4–5 photon photoemission process

be random for every laser shot in a kHz amplified laser system, and any CEP correlation should be destroyed when shifting the tagged CEP list by a single event. When shifting by more events, the modulation becomes less and less pronounced and entirely fades away into random noise after shifting by a number of events corresponding to about 2 s (events are correlated to timing via the count rate). This was consistently found for both measurements shown in Fig. 3 despite their different count rates (~ 1000 counts/s for NPOP vs. ~ 150 counts/s for gold surface roughness hot spots).

The persistence of the observed apparent CEP modulation of the photoelectron spectra over timescales on the order of one second suggests a correlation with slowly varying laser parameters other than its CEP, such as the intensity, which affects both the photoelectron spectrum and the CEP measurement inside the phase meter in a correlated way and thus introduces an apparent CEP artifact into the CEP-tagged measurement. The intensity appears to be a suitable cause for this effect, since intensity fluctuations of our laser take place on a timescale of hundreds of milliseconds and above with an amplitude of 0.6 % rms over 1 min and up to several percent over few hours. This means that on timescales of few hundred milliseconds and below the laser intensity is essentially constant, which is in good agreement with the observed temporal persistence of the apparent CEP modulation. On larger timescales (seconds and above), intensity fluctuations become more pronounced, which destroys any correlation between measured events via the laser intensity.

Figure 4a shows normalized photoemission spectra from the gold surface roughness sample for different relative laser intensities, I_0 being the intensity used for the phase-tagged experiments in Figs. 2f, 3d, f. A space-charge-induced energy shift and an increase in broadening

with increasing laser intensity are clearly visible. Figure 4b quantifies the shift of the peak kinetic energy (blue curve). An onset is evident at about $0.9 I_0$, attributed to space charge, followed by a nearly linear energy shift with intensity. Around I_0 , the energy shift is about 20 meV per % of intensity change. Besides the energy shift, it is worth to note that the count rate increases as a function of intensity with an exponent of 4.4 (red curve), indicating a 4–5 photon photoemission process.

An intensity-dependent energy shift of the photoemission spectrum can only explain the persistent CEP modulation if it is accompanied by an intensity-dependent disbalance of the PAP, which selectively introduces a deviation from a uniform distribution of counts over the CEP for energy spectra that are shifted with respect to the average spectrum due to their intensity dependence. Figure 5a shows the PAPs for different relative intensities, I_0 being again the intensity used for the phase-tagged experiments in Fig. 3d, f. A change in shape as well as in the polar distribution of counts is clearly visible as a function of intensity. The distribution of counts as a function of the polar angle is depicted more clearly in Fig. 5b and is normally used for balancing the PAP (e.g., for the measurements shown in Fig. 3) such that each CEP segment contains the same number of counts. Here, the balancing was omitted in order to show the non-uniform distribution of counts within the PAP. Since the shape shifts and changes with intensity, the CEP retrieval becomes unbalanced for laser intensities other than the intensity at which the PAP for CEP tagging was recorded. This disbalance is quantified as the deviation from unity when normalizing the distribution of counts as a function of CEP at a particular intensity to the distribution at I_0 . The counts distribution curve within the PAP can be obtained for any intensity within the measured range around I_0 by interpolation. Figure 5c shows the resulting disbalance as a function of CEP for an intensity change of 0.6 % around I_0 in black (typical laser intensity drift over 1 min) and 6 % in blue (typical laser intensity drift over few hours), respectively. The disbalance exhibits a periodicity of π and scales approximately linearly with the intensity change. It amounts to ~ 2.3 % peak-to-peak (for 0.6 % intensity change) or ~ 23 % peak-to-peak (for 6 % intensity change), respectively.

In order to reproduce the impact of this disbalance on the measured CEP spectrogram, we performed a phase tagging simulation using 50 million single shots and compared it with the measurement of the gold surface roughness sample. We chose this sample because of the similarity of the corresponding PAP (see Fig. 3e) with the PAP used for the investigation of the intensity dependence (see Fig. 5a, $I/I_0 = 1.00$). The measured CEP spectrogram is shown in Fig. 6a for comparison along with the shift of the central

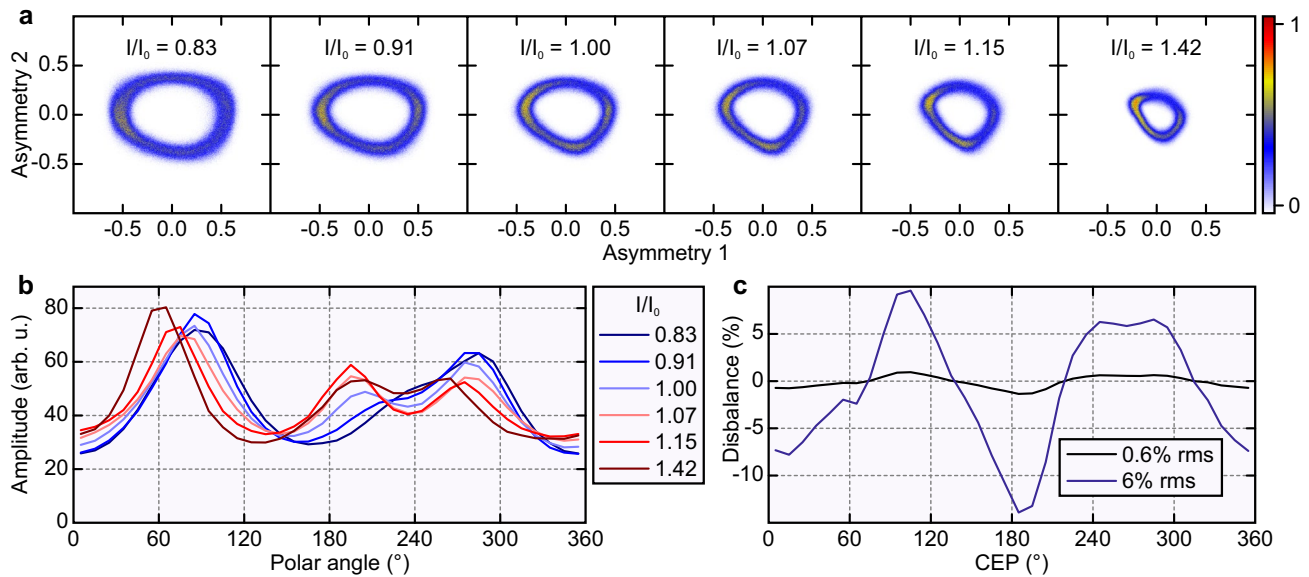


Fig. 5 Laser intensity dependence of the PAP and intensity-induced disbalance of the CEP retrieval. **a** PAP as a function of relative intensity (I/I_0), I_0 being the intensity used for phase-tagged experiments. The *colorbar* shows the counts. **b** Polar distribution of counts,

extracted from the PAP. **c** Calculated disbalance of the CEP retrieval for a laser intensity change of 0.6 % (black) and 6 % (blue), respectively, around I_0

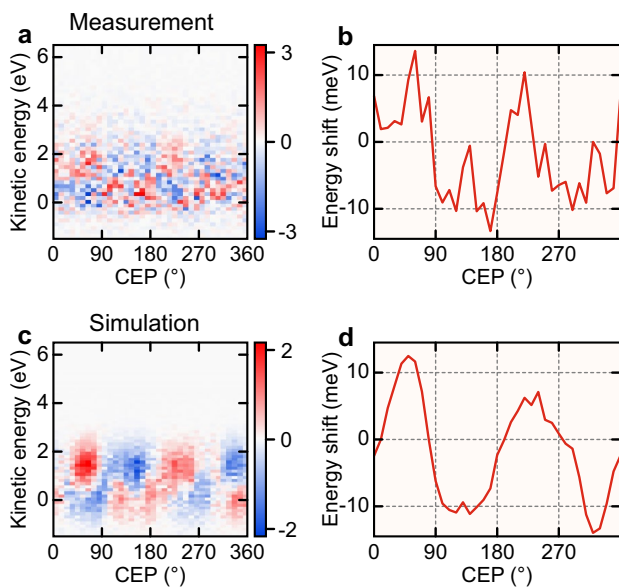


Fig. 6 Simulation of apparent CEP modulation caused by laser intensity fluctuations. **a** Measured normalized CEP spectrogram for the gold surface roughness with the averaged spectrum subtracted. The *colorbar* represents the modulation depth in percent (from Fig. 3f). **b** Central kinetic energy shift as a function of CEP, obtained from the measured spectrogram. **c** Simulated normalized CEP spectrogram with the averaged spectrum subtracted for a Gaussian intensity distribution with a standard deviation of 6 % around I_0 . The *colorbar* represents the modulation depth in percent. See text for simulation details. **d** Central kinetic energy shift as a function of CEP, obtained from the simulated spectrogram

kinetic energy as a function of CEP (Fig. 6b), determined by Gaussian fits.

For simplicity, a Gaussian kinetic energy distribution was chosen for the simulation, resembling the experimentally obtained energy spectrum of the gold surface roughness sample (~ 1.6 eV full width at half maximum, ~ 0.8 eV central energy), as well as a Gaussian intensity distribution around I_0 , the standard deviation being used as a variable parameter (see below), and a random CEP for every event. All distributions (energy, intensity, CEP) were initially uncorrelated. The kinetic energy of each event was then modified according to the associated laser intensity using the experimentally obtained value of 20 meV per % of intensity change (see Fig. 4b). Also, the weighting of each event was calculated according to the disbalance value of its laser intensity and CEP (see Fig. 5c). Afterward, a CEP spectrogram was constructed by summing up the weightings of all events in a particular energy and CEP bin. The standard deviation of the intensity distribution was used as a parameter in the simulation in order to find the best match to the measurement. The CEP spectrogram for a laser intensity distribution of 6 % rms is shown in Fig. 6c along with the shift of the central kinetic energy as a function of CEP (Fig. 6d). This value is in good agreement with the typical laser intensity drift over several hours of measurement time and yields the best match to the measured CEP spectrogram as well as the measured shift of the kinetic energy of about 26 meV peak-to-peak. Despite the different PAPs used for

the measurement and simulation, resulting in qualitatively slightly different shapes, we obtained a remarkable agreement, both qualitatively (matching modulation period of π) and quantitatively (matching modulation depth and energy shift). Since the simulation was performed with no intrinsic CEP effect, i.e., no initial correlation between CEP and kinetic energy or weighting, this result constitutes a strong evidence for laser intensity effects being the cause of the observed apparent CEP modulation.

4 Conclusions

The presented work demonstrates first CEP-tagged ToF-PEEM experiments on nanoplasmonic samples. An intensity-related CEP artifact was discovered in these measurements, which arises from an intensity-dependent energy shift of the photoelectrons emitted from the sample in combination with an intensity-dependent disbalance of the CEP retrieval from a stereographic ATI phase meter. A detailed experimental investigation and analysis of this effect, combined with simulations, confirms modulation depth and periodicity of this CEP artifact, which is caused by laser intensity fluctuations on a timescale of few hundred milliseconds and above. This finding is crucial particularly for the studies of low-probability CEP-dependent processes employing the phase tagging technique, as the artifact might easily outweigh a weak intrinsic CEP modulation of the studied sample. Shortening the measurement time in order to reduce laser intensity fluctuations seems infeasible with typical kHz amplified laser systems, given the low count rates necessary to avoid space charge effects (≤ 1 electron per pulse). Alternatively, CEP-tagged ToF-PEEM measurements have to be restricted to plasmonic samples which exhibit a strong CEP dependence, such that the CEP artifact becomes negligible compared to the intrinsic CEP modulation.

The intensity-related CEP artifact can possibly be remedied by active intensity stabilization at the expense of optical power or by introducing intensity tagging, i.e., recording the intensity for each laser shot in addition to the CEP measurement. The latter is already feasible with the current data acquisition system by adding another channel for single-shot recording of the laser power, e.g., via a photodetector. In postprocessing, the data can then be sorted by intensity and a balanced CEP retrieval can be performed using a correct PAP for each intensity. The identification and elimination of the CEP artifact is a crucial requirement for precise measurements on specially tailored nanostructures using CEP-tagged ToF-PEEM, which will be the next step to control and reveal plasmonic optical fields with an unprecedented spatiotemporal resolution.

Acknowledgments We are grateful to X. Zhou for providing the multicrystalline gold film sample and J. Zou for technical assistance in the experiments. We acknowledge L. Hui, S. Zherebtsov and J. Schötz for support and fruitful discussions. We also acknowledge gratefully the financial support by the German Science Foundation (DFG) through the Cluster of Excellence: Munich Centre for Advanced Photonics (MAP) and the priority program SPP 1391, the Nanosystems Initiative Munich, the TUM-IAS Focus group “Nanophotonics,” the International Graduate School for Science and Engineering (TUM-IGSSE), the IBM International Ph.D. Fellowship Program and the Deanship of Scientific Research at King Saud University through research group no. IRG14-07A.

Open Access This article is distributed under the terms of the Creative Commons Attribution 4.0 International License (<http://creativecommons.org/licenses/by/4.0/>), which permits unrestricted use, distribution, and reproduction in any medium, provided you give appropriate credit to the original author(s) and the source, provide a link to the Creative Commons license, and indicate if changes were made.

References

1. M. Fiess, M. Schultze, E. Goulielmakis, B. Drenth, J. Gagnon, M. Hofstetter, R. Kienberger, F. Krausz, Versatile apparatus for attosecond metrology and spectroscopy. *Rev. Sci. Instrum.* **81**(9), 093103 (2010)
2. E. Magerl, S. Neppl, A.L. Cavalieri, E.M. Bothschafter, M. Stanislowski, T. Uphues, M. Hofstetter, U. Kleineberg, J.V. Barth, D. Menzel, F. Krausz, R. Ernstorfer, R. Kienberger, P. Feulner, A flexible apparatus for attosecond photoelectron spectroscopy of solids and surfaces. *Rev. Sci. Instrum.* **82**(6), 063104 (2011)
3. L. Xu, T.W. Hänsch, C. Spielmann, A. Poppe, T. Brabec, F. Krausz, Route to phase control of ultrashort light pulses. *Opt. Lett.* **21**(24), 2008–2010 (1996)
4. F.W. Helbing, G. Steinmeyer, U. Keller, R.S. Windeler, J. Stenger, H.R. Telle, Carrier-envelope offset dynamics of mode-locked lasers. *Opt. Lett.* **27**(3), 194–196 (2002)
5. T. Udem, R. Holzwarth, T.W. Hänsch, Optical frequency metrology. *Nature* **416**(6877), 233–237 (2002)
6. A. Baltuska, T. Udem, M. Uiberacker, M. Hentschel, E. Goulielmakis, C. Gohle, R. Holzwarth, V.S. Yakovlev, A. Scrinzi, T.W. Hänsch, F. Krausz, Attosecond control of electronic processes by intense light fields. *Nature* **421**(6923), 611–615 (2003)
7. G. Sansone, E. Benedetti, F. Calegari, C. Vozzi, L. Avaldi, R. Flammini, L. Poletto, P. Villoresi, C. Altucci, R. Velotta, S. Stagira, S. De Silvestri, M. Nisoli, Isolated single-cycle attosecond pulses. *Science* **314**(5798), 443–446 (2006)
8. N.G. Johnson, O. Herrwerth, A. Wirth, S. De, I. Ben-Itzhak, M. Lezius, B. Bergues, M.F. Kling, A. Sennleber, C.D. Schroeter, R. Moshhammer, J. Ullrich, K.J. Betsch, R.R. Jones, A.M. Saylor, T. Rathje, K. Rühle, W. Mueller, G.G. Paulus, Single-shot carrier-envelope-phase-tagged ion-momentum imaging of nonsequential double ionization of argon in intense 4-fs laser fields. *Phys. Rev. A* **83**(1), 013412 (2011)
9. M. Kuebel, A.S. Alnaser, B. Bergues, T. Pischke, J. Schmidt, Y. Deng, C. Jendrzejewski, J. Ullrich, G.G. Paulus, A.M. Azzeer, U. Kleineberg, R. Moshhammer, M.F. Kling, Strong-field control of the dissociative ionization of N_2O with near-single-cycle pulses. *New J. Phys.* **16**(6), 065017 (2014)
10. X. Liu, H. Rottke, E. Eremina, W. Sandner, E. Goulielmakis, K.O. Keeffe, M. Lezius, F. Krausz, F. Lindner, M.G. Schatzel, G.G. Paulus, H. Walther, Nonsequential double ionization at

- the single-optical-cycle limit. *Phys. Rev. Lett.* **93**(26), 263001 (2004)
11. A.S. Alnaser, M. Kuebel, R. Siemering, B. Bergues, N.G. Kling, K.J. Betsch, Y. Deng, J. Schmidt, Z.A. Alahmed, A.M. Azzeer, J. Ullrich, I. Ben-Itzhak, R. Moshhammer, U. Kleineberg, F. Krausz, R. de Vivie-Riedle, M.F. Kling, Subfemtosecond steering of hydrocarbon deprotonation through superposition of vibrational modes. *Nat. Commun.* **5**, 3800 (2014)
 12. H. Li, B. Mignolet, G. Wachter, S. Skruszewicz, S. Zherebtsov, F. Sussmann, A. Kessel, S.A. Trushin, N.G. Kling, M. Kübel, B. Ahn, D. Kim, I. Ben-Itzhak, C.L. Cocke, T. Fennel, J. Tiggesbäumker, K.-H. Meiwes-Broer, C. Lemell, J. Burgdörfer, R.D. Levine, F. Remacle, M.F. Kling, Coherent electronic wave packet motion in C60 controlled by the waveform and polarization of few-cycle laser fields. *Phys. Rev. Lett.* **114**(12), 123004 (2015)
 13. A. Apolonski, P. Dombi, G.G. Paulus, M. Kakehata, R. Holzwarth, T. Udem, C. Lemell, K. Torizuka, J. Burgdoerfer, T.W. Haensch, F. Krausz, Observation of light-phase-sensitive photoemission from a metal. *Phys. Rev. Lett.* **92**(7), 073902 (2004)
 14. P. Dombi, A. Apolonski, C. Lemell, G.G. Paulus, M. Kakehata, R. Holzwarth, T. Udem, K. Torizuka, J. Burgdörfer, T.W. Hänsch, F. Krausz, Direct measurement and analysis of the carrier-envelope phase in light pulses approaching the single-cycle regime. *New J. Phys.* **6**(1), 39 (2004)
 15. M. Krüger, M. Schenk, P. Hommelhoff, Attosecond control of electrons emitted from a nanoscale metal tip. *Nature* **475**(7354), 78–81 (2011)
 16. S. Zherebtsov, T. Fennel, J. Plenge, E. Antonsson, I. Znakovskaya, A. Wirth, O. Herrwerth, F. Suszmann, C. Peltz, I. Ahmad, S.A. Trushin, V. Pervak, S. Karsch, M.J.J. Vrakking, B. Langer, C. Graf, M.I. Stockman, F. Krausz, E. Ruhl, M.F. Kling, Controlled near-field enhanced electron acceleration from dielectric nanospheres with intense few-cycle laser fields. *Nat. Phys.* **7**(8), 656–662 (2011)
 17. P. Dombi, P. Rácz, Ultrafast monoenergetic electron source by optical waveform control of surface plasmons. *Opt. Express* **16**(5), 2887–2893 (2008)
 18. P. Dombi, S.E. Irvine, P. Rácz, M. Lenner, N. Kroó, G. Farkas, A. Mitrofanov, A. Baltuška, T. Fuji, F. Krausz, A.Y. Elezzabi, Observation of few-cycle, strong-field phenomena in surface plasmon fields. *Opt. Express* **18**(23), 24206–24212 (2010)
 19. S.E. Irvine, P. Dombi, G. Farkas, A.Y. Elezzabi, Influence of the carrier-envelope phase of few-cycle pulses on ponderomotive surface-plasmon electron acceleration. *Phys. Rev. Lett.* **97**(14), 146801 (2006)
 20. B. Piglosiewicz, S. Schmidt, D.J. Park, J. Vogelsang, P. Grosz, C. Manzoni, P. Farinello, G. Cerullo, C. Lienau, Carrier-envelope phase effects on the strong-field photoemission of electrons from metallic nanostructures. *Nat. Photonics* **8**(1), 37–42 (2014)
 21. L. Gierster, A.A. Ünal, L. Pape, F. Radu, F. Kronast, Laser induced magnetization switching in a TbFeCo ferrimagnetic thin film: discerning the impact of dipolar fields, laser heating and laser helicity by XPEEM. *Ultramicroscopy* **159**(Part 3), 508–512 (2015)
 22. T. Nakagawa, K. Watanabe, Y. Matsumoto, T. Yokoyama, Magnetic circular dichroism photoemission electron microscopy using laser and threshold photoemission. *J. Phys.: Condens. Matter* **21**(31), 314010 (2009)
 23. J. Vogel, W. Kuch, M. Bonfim, J. Camarero, Y. Pennec, F. Offi, K. Fukumoto, J. Kirschner, A. Fontaine, S. Pizzini, Time-resolved magnetic domain imaging by x-ray photoemission electron microscopy. *Appl. Phys. Lett.* **82**(14), 2299–2301 (2003)
 24. G.H. Fecher, O. Schmidt, Y. Hwu, G. Schönhense, Multiphoton photoemission electron microscopy using femtosecond laser radiation. *J. Electron Spectrosc. Relat. Phenom.* **126**, 77–87 (2002)
 25. M. Aeschlimann, M. Bauer, D. Bayer, T. Brixner, S. Cunovic, F. Dimler, A. Fischer, W. Pfeiffer, M. Rohmer, C. Schneider, F. Steeb, C. Strüber, D.V. Voronine, Spatiotemporal control of nanooptical excitations. *Proc. Natl. Acad. Sci.* **107**(12), 5329–5333 (2010)
 26. A. Kubo, K. Onda, H. Petek, Z. Sun, Y.S. Jung, H.K. Kim, Femtosecond imaging of surface plasmon dynamics in a nanostructured silver film. *Nano Lett.* **5**(6), 1123–1127 (2005)
 27. E. Mårzell, C.L. Arnold, E. Lorek, D. Guenot, T. Fordell, M. Miranda, J. Mauritsson, H. Xu, A. L’Huillier, A. Mikkelsen, Secondary electron imaging of nanostructures using extreme ultraviolet attosecond pulse trains and infra-red femtosecond pulses. *Ann. Phys.* **525**(1–2), 162–170 (2013)
 28. F.-J. Meyer zu Heringdorf, L.I. Chelaru, S. Möllenbeck, D. Thien, M. Horn-von Hoegen, Femtosecond photoemission microscopy. *Surf. Sci.* **601**(20), 4700–4705 (2007)
 29. A. Mikkelsen, J. Schwenke, T. Fordell, G. Luo, K. Klünder, E. Hilner, N. Anttu, A.A. Zakharov, E. Lundgren, J. Mauritsson, J.N. Andersen, H.Q. Xu, A. L’Huillier, Photoemission electron microscopy using extreme ultraviolet attosecond pulse trains. *Rev. Sci. Instrum.* **80**(12), 123703 (2009)
 30. S.H. Chew, F. Süßmann, C. Späth, A. Wirth, J. Schmidt, S. Zherebtsov, A. Guggenmos, A. Oelsner, N. Weber, J. Kapaldo, A. Glierin, M.I. Stockman, M.F. Kling, U. Kleineberg, Time-of-flight-photoelectron emission microscopy on plasmonic structures using attosecond extreme ultraviolet pulses. *Appl. Phys. Lett.* **100**(5), 051904 (2012)
 31. J. Lin, N. Weber, A. Wirth, S.H. Chew, M. Escher, M. Merkel, M.F. Kling, M.I. Stockman, F. Krausz, U. Kleineberg, Time of flight-photoemission electron microscope for ultrahigh spatiotemporal probing of nanoplasmonic optical fields. *J. Phys.: Condens. Matter* **21**(31), 314005 (2009)
 32. M.I. Stockman, M.F. Kling, U. Kleineberg, F. Krausz, Attosecond nanoplasmonic-field microscope. *Nat. Photonics* **1**(9), 539–544 (2007)
 33. R. Holzwarth, T. Udem, T.W. Hänsch, J.C. Knight, W.J. Wadsworth, P.S.J. Russell, Optical frequency synthesizer for precision spectroscopy. *Phys. Rev. Lett.* **85**(11), 2264–2267 (2000)
 34. D.J. Jones, S.A. Diddams, J.K. Ranka, A. Stentz, R.S. Windeler, J.L. Hall, S.T. Cundiff, Carrier-envelope phase control of femtosecond mode-locked lasers and direct optical frequency synthesis. *Science* **288**(5466), 635–639 (2000)
 35. C. Li, E. Moon, H. Wang, H. Mashiko, C.M. Nakamura, J. Tackett, Z. Chang, Determining the phase-energy coupling coefficient in carrier-envelope phase measurements. *Opt. Lett.* **32**(7), 796–798 (2007)
 36. T. Rathje, N.G. Johnson, M. Möller, F. Süßmann, D. Adolph, M. Kübel, R. Kienberger, M.F. Kling, G.G. Paulus, A.M. Saylor, Review of attosecond resolved measurement and control via carrier-envelope phase tagging with above-threshold ionization. *J. Phys. B: At. Mol. Opt. Phys.* **45**(7), 074003 (2012)
 37. A.M. Saylor, T. Rathje, W. Müller, C. Kürbis, K. Rühle, G. Stibenz, G.G. Paulus, Real-time pulse length measurement of few-cycle laser pulses using above-threshold ionization. *Opt. Express* **19**(5), 4464–4471 (2011)
 38. T. Wittmann, B. Horvath, W. Helml, M.G. Schatzel, X. Gu, A.L. Cavalieri, G.G. Paulus, R. Kienberger, Single-shot carrier-envelope phase measurement of few-cycle laser pulses. *Nat. Phys.* **5**(5), 357–362 (2009)
 39. M. Kuebel, K.J. Betsch, N.G. Johnson, U. Kleineberg, R. Moshhammer, J. Ullrich, G.G. Paulus, M.F. Kling, B. Bergues, Carrier-envelope-phase tagging in measurements with long acquisition times. *New J. Phys.* **14**(9), 093027 (2012)
 40. P. Rácz, S.E. Irvine, M. Lenner, A. Mitrofanov, A. Baltuška, A.Y. Elezzabi, P. Dombi, Strong-field plasmonic electron acceleration with few-cycle, phase-stabilized laser pulses. *Appl. Phys. Lett.* **98**(11), 111116 (2011)

41. Y.-Y. Yang, A. Scrinzi, A. Husakou, Q.-G. Li, S.L. Stebbings, F. Stüßmann, H.-J. Yu, S. Kim, E. Rühl, J. Herrmann, X.-C. Lin, M.F. Kling, High-harmonic and single attosecond pulse generation using plasmonic field enhancement in ordered arrays of gold nanoparticles with chirped laser pulses. *Opt. Express* **21**(2), 2195–2205 (2013)
42. A. Oelsner, M. Rohmer, C. Schneider, D. Bayer, G. Schönhense, M. Aeschlimann, Time- and energy resolved photoemission electron microscopy-imaging of photoelectron time-of-flight analysis by means of pulsed excitations. *J. Electron Spectrosc. Relat. Phenom.* **178–179**, 317–330 (2010)
43. D.B. Milošević, G.G. Paulus, W. Becker, High-order above-threshold ionization with few-cycle pulse: a meter of the absolute phase. *Opt. Express* **11**(12), 1418–1429 (2003)
44. G.G. Paulus, F. Lindner, H. Walther, A. Baltuška, E. Goulielmakis, M. Lezius, F. Krausz, Measurement of the phase of few-cycle laser pulses. *Phys. Rev. Lett.* **91**(25), 253004 (2003)
45. A.M. Sayler, T. Rathje, W. Müller, K. Rühle, R. Kienberger, G.G. Paulus, Precise, real-time, every-single-shot, carrier-envelope phase measurement of ultrashort laser pulses. *Opt. Lett.* **36**(1), 1–3 (2011)
46. P. Nordlander, E. Prodan, Plasmon hybridization in nanoparticles near metallic surfaces. *Nano Lett.* **4**(11), 2209–2213 (2004)
47. A. Rueda, M. Stemmler, R. Bauer, K. Müllen, Y. Fogel, M. Kreiter, Optical resonances of gold nanoparticles on a gold surface: quantitative correlation of geometry and resonance wavelength. *New J. Phys.* **10**(11), 113001 (2008)
48. F. Schertz, M. Schmelzeisen, R. Mohammadi, M. Kreiter, H.-J. Elmers, G. Schönhense, Near field of strongly coupled plasmons: uncovering dark modes. *Nano Lett.* **12**(4), 1885–1890 (2012)
49. J.-S. Huang, V. Callegari, P. Geisler, C. Brüning, J. Kern, J.C. Prangma, X. Wu, T. Feichtner, J. Ziegler, P. Weinmann, M. Kamp, A. Forchel, P. Biagioni, U. Sennhauser, B. Hecht, Atomically flat single-crystalline gold nanostructures for plasmonic nanocircuitry. *Nat. Commun.* **1**, 150 (2010)
50. F. Schertz, M. Schmelzeisen, M. Kreiter, H.-J. Elmers, G. Schönhense, Field emission of electrons generated by the near field of strongly coupled plasmons. *Phys. Rev. Lett.* **108**(23), 237602 (2012)
51. L.V. Keldysh, Ionization in the field of a strong electromagnetic wave. *J. Exp. Theor. Phys.* **20**(5), 1307 (1965)